RSC Advances

ROYAL SOCIETY OF CHEMISTRY

www.rsc.org/advances

Structure, luminescence property and abnormal energy transfer behavior of color-adjustable $Ca_3Hf_2SiAl_2O_{12}:Ce^{3+}$, Mn^{2+} phosphors

Xin Ding, Wanying Geng, Qian Wang, Yuhua Wang*

Department of Materials Science, School of Physical Science and Technology, Lanzhou University

Key Laboratory of Special Function Materials and Structure Design, Ministry of Education,

Lanzhou University, Tianshui South Road No. 222, Lanzhou, Gansu 730000, PR China

Abstract

A series of color-adjustable phosphors $Ca_3Hf_2SiAl_2O_{12}:Ce^{3+}$, Mn^{2+} were synthesized through a high temperature solid-state method. $Ca_3Hf_2SiAl_2O_{12}$ belongs to body-centered cubic crystal system and Ia-3d (230) space-group. It was found that three different cation sites in the $Ca_3Hf_2SiAl_2O_{12}$ phase were occupied evenly by Ce^{3+} and Mn^{2+} ions. Different situation of Mn^{2+} occupying sites and energy transfer from Ce^{3+} to Mn^{2+} can appear with different Mn^{2+} content and the critical distance was calculated to be R_{c1}=10.8 Å, R_{c2}=10.1 Å and R_{c3}=12.6 Å after calculation of energy transfer from the Ce^{3+} to Mn^{2+} by using the concentration quenching method. $Ca_3Hf_2SiAl_2O_{12}$: Ce^{3+}, Mn^{2+} phosphors exhibited a broad excitation band ranging from 300 to 450 nm and two broad asymmetric emission bands upon 400 nm excitation. The emission colors of $Ca_3Hf_2SiAl_2O_{12}:Ce^{3+}$, Mn^{2+} could be tuned from blue-green (0.2303, 0.3265) to white (0.3350, 0.3388) by changing the ratio of Ce^{3+}/Mn^{2+}. The correlated color temperature can be adjusted from 12763 K to 5379 K. It indicated that $Ca_3Hf_2SiAl_2O_{12}:Ce^{3+}$, Mn^{2+} possesses potential applications in white-LEDs.

*Corresponding author at: Department of Materials Science, School of Physical Science and Technology, Lanzhou University, Lanzhou, 730000, PR China.

Tel.: +86 931 8912772; fax: +86 931 8913554.

Corresponding author' email: wyh@lzu.edu.cn

1. Introduction

Nowadays, white light emitting diodes (W-LEDs) have attracted considerable attention and been used in many areas [1] for their various advantages such as small volume, high efficiency, long lifetime, energy saving and environment-friendly [2, 3]. The initial method to get W-LED lamp is consisting three triple LED chips for red, green and blue [4]. Though it is easy to fabricate, it has different thermal stability, different drive voltage, different degradation and expensive for different LED chips [5-7], which restrains its application. Another feasible scheme for W-LED generation is using blue or ultraviolet chips combining with some phosphors which can be excited by them. For instance, YAG: Ce^{3+} yellow phosphor excited by a blue InGaN chip can generate white light by yellow emission from the phosphor and blue light from the chip. Though it has been commercialization and widely used, it cannot satisfy the optimum requirements. Different degradation for blue chip and phosphor leads to chromatic aberration. Lack of red light component causes high correlated color temperature (7765K) and poor color rendering index which restricts its more broad applications. In order to obtain warm white light and high color rendering index, red phosphor is introduced to that system [8-12]. In addition to this method, another kind of W-LEDs can be fabricated by combing of the GaN-based blue chip with green and red phosphors or via coupling ultraviolet (UV) LED (350–420 nm) with blue, green and red phosphors [13-15]. As compared to YAG: Ce^{3+} yellow phosphor excited by a blue InGaN chip, this type of W-LEDs

has low correlated color temperature and high color rendering index (Ra > 90), but low luminous efficiency due to the re-absorption between phosphors. Recently, more efforts to get satisfied warm white light have been focused on by using single-component phosphor which can emit white light doped with rare earth ions [16-23]. The single-component phosphor is more stable, more efficient and no phase separation, which can avoid the above mentioned problems. The single-composition white-light phosphor can be realized by co-doping a sensitizer and an activator such as Ce^{3+} and Mn^{2+} into the same host. It is accepted that the Ce^{3+} ion with the 4f configuration in solids shows efficient broad band luminescence due to the 4f– 5d parity allowed electric dipole transition. Attributing to the extended radial wavefunctions of the 5d state, the Ce^{3+} ion usually has a large Stokes shift and its emission can be shifted from UV to the visible region of the electromagnetic spectrum, which is dependent on the host lattice. Moreover, the Ce^{3+} ion also acts as a good sensitizer, transferring a part of its energy to the activator ion. Being considered as a candidate of the activator, the transition-metal ion Mn^{2+} can give a broad emission band in the visible range, and the emission color of Mn^{2+} can vary from green to red, which is strongly affected by the crystal field of the host materials. Owing to the forbidden $^4T_1$–$^6A_1$ transition of Mn^{2+} ion, the emission intensity of a Mn^{2+}-ion singly doped phosphor is low under UV excitation. Based on the above-mentioned considerations, it is necessary to enhance the emission intensity of Mn^{2+}-doped materials by introducing an efficient sensitizer Ce^{3+}. More importantly, white light can be obtained by co-doping Ce^{3+} and Mn^{2+} ions under effective resonance-type energy transfer in a single phase host. Therefore, a single-phase white-light-emitting phosphor based on the mechanism of energy transfer has been realized by doping the sensitizers and activators in some host lattices such as $Ca_3Sc_2Si_3O_{12}$: Ce^{3+}, Mn^{2+} [24], $Ba_2Li_2Si_2O_7$: Ce^{3+}, Mn^{2+} [25], $Ca_2Gd_8Si_6O_{26}$: Ce^{3+}, Mn^{2+} [26], $Ca_3YGa_3B4O_{15}$: Ce^{3+}, Mn^{2+} [27].

A new species of the garnet super-group $Ca_3(Hf, Sn, Zr, Ti)_2SiAl_2O_{12}$ was discovered in metasomatically altered carbonate-silicate xenoliths in ignimbrites of the upper Chegem Caldera, Northern Caucasus, Kabardino-Balkaria, Russia at 2013. It is said that Hf-garnet obtains higher in the conduction band, above 4.0 eV, which may obtain NUV excitation. We previously reported the discovery and crystal structure of $Ca_3Hf_2SiAl_2O_{12}$ (hereafter referred to as CHSA) and explored the potential of its Ce^{3+}-activated derivative for use as a phosphor in LED. CHSA: Ce^{3+} emits a strong blue-green light under excitation from the UV to near-UV. Here, we reported Ce^{3+}, Mn^{2+} co-doped CHSA and studied its energy transfer situation. According to changing different Mn^{2+} contents, we realized the adjustable CIE coordinates and color temperature.

2. Experimental Section

$CaCO_3$ (99.9%), HfO_2 (99.99%), $Al(OH)_3$ (AR), H_2SiO_3 (AR), CeO_2 (99.99%) and $MnCO_3$ (99.9%) as the raw materials are stoichiometric and 5wt% H_3BO_3 as the flux is also used in the synthesis process. Aluminum oxide crucibles (10 mm*10 mm) and porcelain boat are utensils for sintering.

2.2 Synthesis

A series of $Ca_3Hf_2SiAl_2O_{12}$: Ce^{3+}, Mn^{2+} samples are synthesized by two-step traditional high temperature solid-stated reaction. The relative amounts of materials are calculated and then are weighed by electronic balance accurate to 4 decimal places. All the raw materials and the flux are put into agate mortar with 8 mL ethanol added in it at the same time. Grind the mixture for 30 min until they are evenly blended and homogeneous. After the mixture dry, transfer the mixture into aluminum oxide crucibles (10 mm*10 mm) and pre-fire at 800 °C for 2 h under air atmosphere,

then, calcine them at 1480 °C for 5 h under flowing 95% N_2−5% H_2 atmosphere in the horizontal tube furnace. When they are cooled with 5 °C /min speed to room temperature, grind them to powders, yielding the resulting phosphor powder.

2.3 Characterization

The phase formation and crystal structure were analyzed by the X-ray powder diffraction (XRD) (D2 PHASER X-ray Diffractometer ,Germany) with graphite monochromator using Cu Kα radiation（λ = 1.54056 A), operating at 30 kV and 15 mA. The investigation range is 10 ^{o} to 80 ^{o} with scanning speed of 15 ^{o} 2θ min^{-1} for the series $Ca_3Hf_2SiAl_2O_{12}:Mn^{2+}$ samples. The photoluminescence (PL) and photoluminescence excitation (PLE) spectra of the samples are measured by a Fluorlog-3 spectrofluorometer equipped with 450 W xenon lamps (Horiba Jobin Yvon). The temperature-dependence luminescence properties are measured on the same spectrophotometer, which is combined with a self-made heating attachment and a computer-controlled electric furnace from room temperature (25 °C) to 250 °C with a heating rate of 100 °C/min and a holding time of 5 min for each temperature point. The luminescence decay curves were obtained by FLS-920T fluorescence spectrophotometer as well. All the testes are carried out at room temperature.

3. Results and Discussion

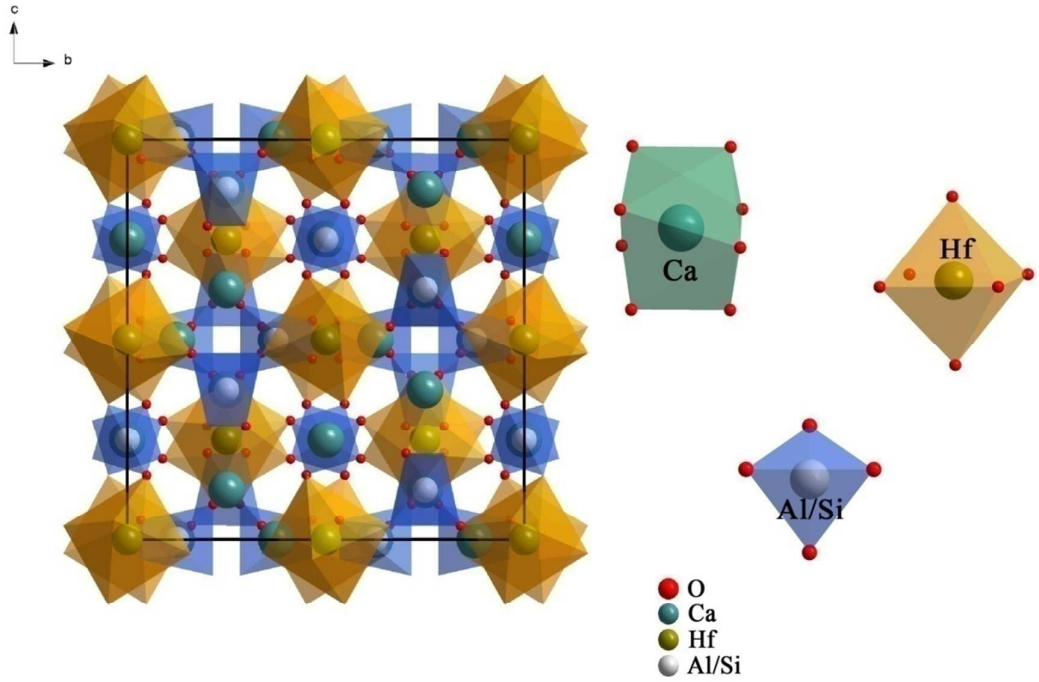

Figure 1 The structure of $Ca_3Hf_2SiAl_2O_{12}$ and the coordination of Ca, Hf and Al/Si

$Ca_3Hf_2SiAl_2O_{12}$ belongs to body-centered cubic crystal system and Ia-3d (230) space-group which is shown in Figure 1 observing from [100] crystal orientation. There are three sites for cations in this crystal structure and only one lattice site for Hf, Al/Si and Ca, respectively. In the present work, there is valency imposed double site-occupancy (R^{4+}, R^{3+}) at the Al/Si tetrahedron site [28, 29], which Al and Si atoms are in substitutional disorder, and the atomic position and anisotropic displacement parameters of Al and Si are constrained to be identical at Al/Si sites in the initial refinements. The yellow octahedrons (six coordination), $[HfO_8]^{4-}$ is fully occupied by Hf, while the blue tetrahedrons site, $[AlO_4]^{5-}$, $[SiO_4]^{4-}$ is occupied by 2/3 Al and 1/3 Si. The green spheres

located in the space between the polyhedrons represent the Ca site. The anion sites (oxygen sites) are located at the shared corners of the octahedra and tetrahedra. According to ions radius analysis, the radius of Ce^{3+} in eight coordinated is 1.283 Å which is close to Ca^{2+} 1.26 Å. It may provide a proof that Ce^{3+} will occupy Ca^{2+} site in this crystal structure. In the same time, the radius of Al^{3+}/Si^{4+} in tetrahedron site is 0.53/0.40 Å and the radius of Hf^{4+} in octahedrons (six coordination) is 0.85 Å. Generally, the radius of Mn^{2+} is larger than Al^{3+}/Si^{4+} and small but close to Hf^{4+}, while smaller than Ca^{2+}. It is considered that Mn^{2+} may occupy every cation site in this structure.

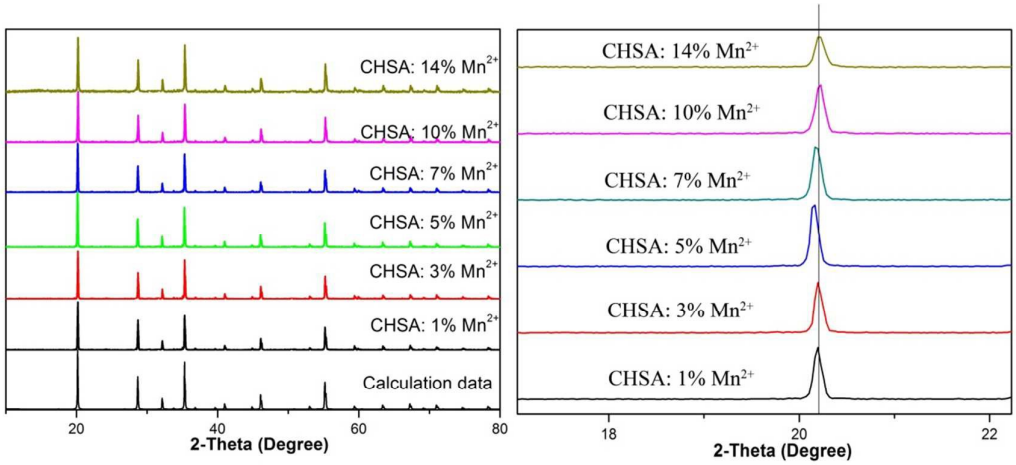

Figure 2 XRD patterns of series $Ca_3Hf_2SiAl_2O_{12}$: $x\%Mn^{2+}$ and calculated data (left image); Peak shift of series XRD patterns (right image)

XRD patterns of the as-prepared CHSA: $y\%Mn^{2+}$ ($1 \leq y \leq 14$) phosphors were collected to verify the phase purity. As given in Figure 2, it can be seen that all the diffraction peaks of the samples can be indexed to the corresponding calculated data basically, suggesting that CHSA: $y\%Mn^{2+}$ with different Mn^{2+} contents can be formed in the single-phased structure. From the right image, the peak shift of series XRD patterns, we can see that the peaks shift to smaller angle firstly with increasing Mn^{2+} content, and then shift to larger angle. It could provide a proof that Mn^{2+} can occupy not only one site. According to analysis above, in the low Mn^{2+} content, Mn^{2+} could occupy Al^{3+}/Si^{4+} tetrahedrons site. The radius of Mn^{2+} in tetrahedrons is 0.80 Å, larger than Al^{3+}/Si^{4+}. According to $2d\sin\theta = n\lambda$, with the interplanar spacing (d) increasing, the sinθ will decrease and lead to the XRD peaks shift to smaller angle. With the increasing of Mn^{2+} content, Mn^{2+} will occupy Hf^{4+} or Ca^{2+} site. The radius of Mn^{2+} in six or eight coordination is smaller than Hf^{4+} or Ca^{2+}. When Mn^{2+} substitutes Hf^{4+} or Ca^{2+}, the interplanar spacing (d) will decrease and lead to XRD peaks shift to larger angle. The phenomenon of peaks shift could be as evidence for Mn^{2+} different occupying situation and it indicates that Mn^{2+} could substitute Al^{3+}/Si^{4+} site. However, it cannot distinguish which site of Hf^{4+} and Ca^{2+} will be occupied by Mn^{2+}. Another situation is that Mn^{2+} may substitute both Hf^{4+} and Ca^{2+}. Because of the radius of Hf^{4+} and Ca^{2+} are both larger than Mn^{2+}. Occupying one site of Hf^{4+} and Ca^{2+} or both sites of them will both lead to peak shift to larger angle.

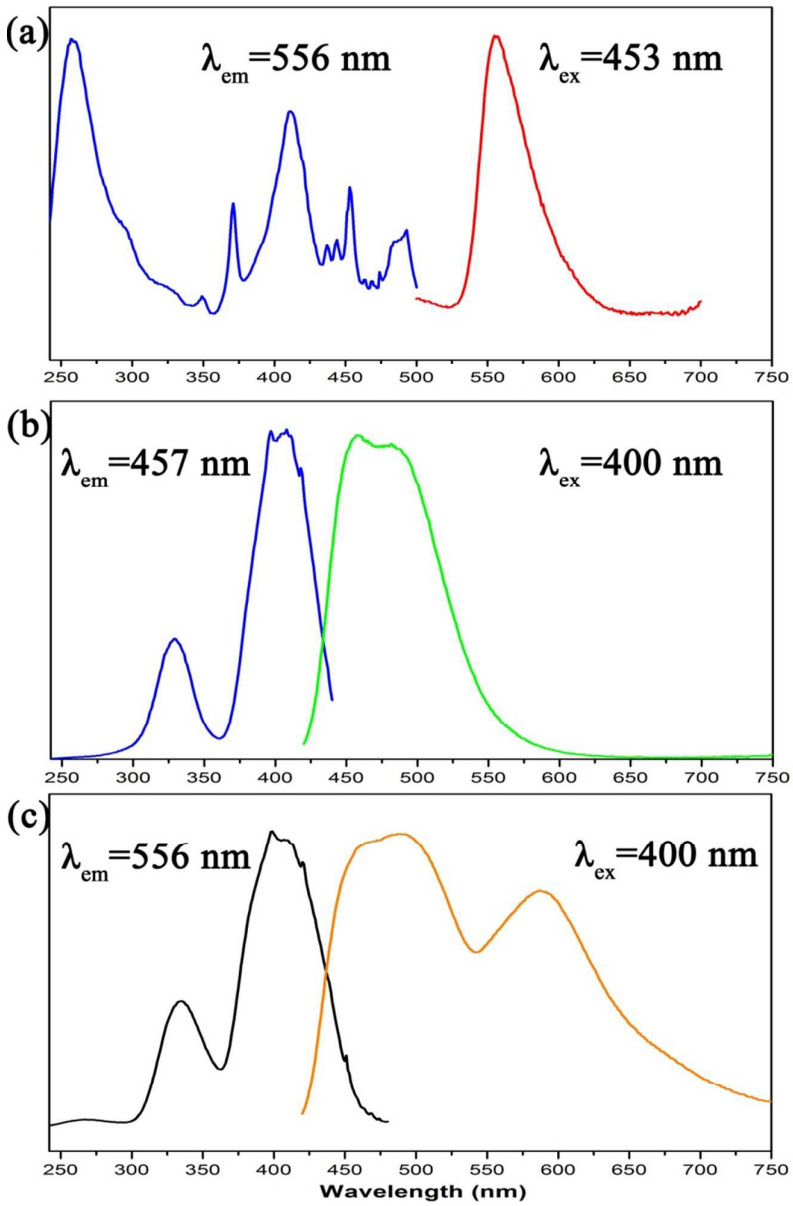

Figure 3 PLE (left) and PL (right) spectra of $Ca_3Hf_2SiAl_2O_{12}$: Mn^{2+} (a); $Ca_3Hf_2SiAl_2O_{12}$: Ce^{3+} (b); $Ca_3Hf_2SiAl_2O_{12}$: Ce^{3+}, Mn^{2+} (c);

Fig. 3 presents the excitation and emission spectra of single doped and co-doped $Ca_3Hf_2SiAl_2O_{12}$ phosphors. As shown in Fig. 3a demonstrates the PLE and PL spectra of CHSA: 1%Mn^{2+}. The excitation spectrum consists of several bands centering at 362nm, 410 nm, 455 nm and 480 nm, corresponding to the transitions of Mn^{2+} ion from ground level $^6A_1(^6S)$ to $^4E(^4D)$, $^4T_2(^4D)$, [$^4A_1(^4G)$, $^4E(^4G)$], and $^4T_1(^4G)$ levels, respectively. The broad emission band from 525 to 600 nm centered at 556 nm ascribed to the spin-forbidden $^4T_1(^4G)$–$^6A_1(^6S)$ transition of the Mn^{2+} ions [30]. The PLE and PL spectra of CHSA: 1%Ce^{3+} sample are shown in Fig. 3b. The PLE spectrum monitored by 457 nm exhibits two distinct excitation bands at 325 and 400 nm, which could be ascribed to the electronic transitions from the ground state to the different crystal field splitting bands of excited 5d states of Ce^{3+}. Upon 400 nm excitation, the PL spectrum consists of an asymmetric broad emission band from 450 to 550 nm with a maximum at 455 nm which is

assigned to the 5d–4f transitions of Ce^{3+}. It is well-known that the typical emission of Ce^{3+} should consist of a double band in view of the transitions of Ce^{3+} ions from 5d state to the $^2F_{5/2}$ and $^2F_{7/2}$ ground states, and the theoretical energy difference of this splitting between $^2F_{5/2}$ and $^2F_{7/2}$ level is about 2000 cm [31].As seen in Fig. 3a and b the significant spectral overlap occurs between the emission band of Ce^{3+} and the excitation band of Mn^{2+}, which indicates the possible resonance type energy transfer from the Ce^{3+} to Mn^{2+} ions in CHSA matrix. The PLE and PL spectra of CHSA: 1%Ce^{3+}, 1%Mn^{2+} monitored at the emission of Mn^{2+} (556 nm) with 400 nm excitation are shown in Figure 3c. Upon excitation at 400 nm, the PL spectrum of CHSA: 1%Ce^{3+}, 1%Mn^{2+} phosphor appears not only as a blue-green band of Ce^{3+} ions also as a green band of the Mn^{2+} ions.

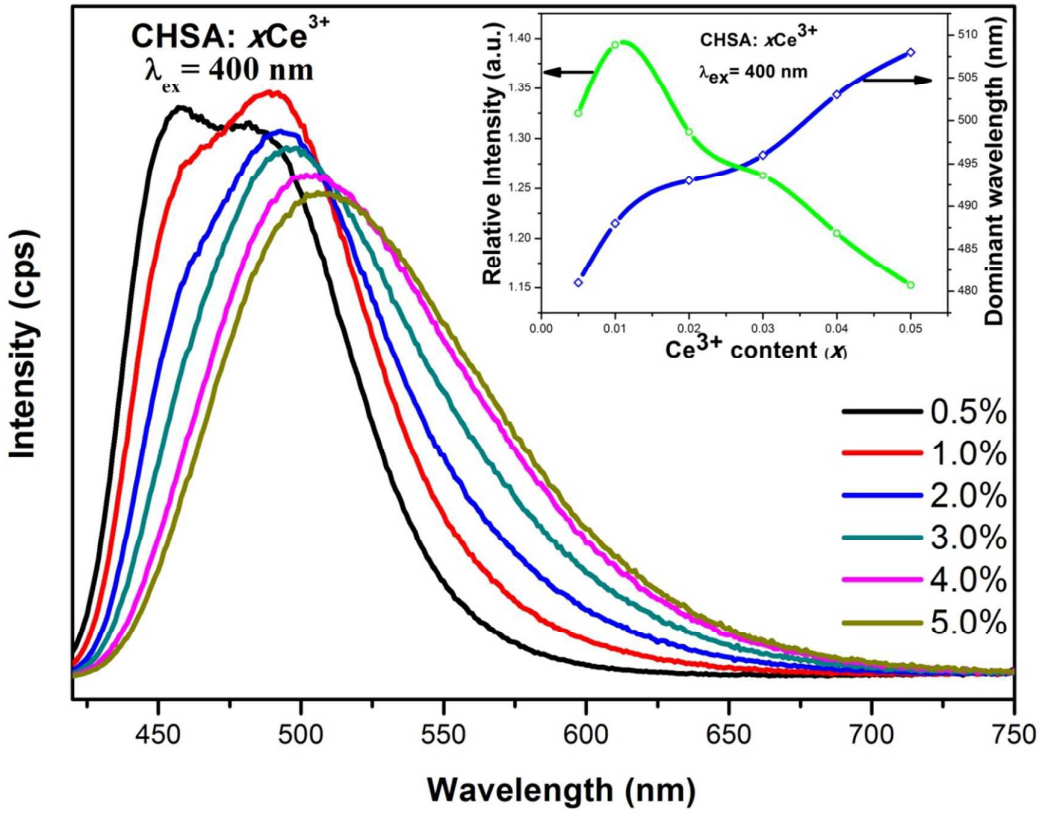

Figure 4 PL properties under 400 nm excitation of series $Ca_3Hf_2SiAl_2O_{12}$: x%Ce^{3+} phosphors; Inset: (Upper right) Dependence of emission intensity and peak position of $Ca_3Hf_2SiAl_2O_{12}$: x%Ce^{3+} phosphors on Ce^{3+} content

From Figure 4, we can see that CHSA: $x$$Ce^{3+}$ can emit cyan light (450-550 nm) under UV excitation and the emission spectra consist of two apparent asymmetric broad peaks before x =0.03 which corresponds to the 5*d*–4*f* allowed transition of Ce^{3+}, beyond x =0.03, emission spectra turn to be a broad peak. Additionally, the inset (upper right) of Figure 4 shows the Ce^{3+} content dependent emission intensity and peak position. It can be easily seen that the emission intensities have an obvious increasing trend with increasing Ce^{3+} concentration, and maximizes at x = 0.01, then the emission intensity decreases. The peak position has apparent red shift from 481 to 508 nm about 1105 cm^{-1}. It is well-known that the typical emission of Ce^{3+} should consist of a double band in view of the transitions of Ce^{3+} ions from 5*d* state to the $^2F_{5/2}$ and $^2F_{7/2}$ ground states. That's the reason why emission spectra consist of two apparent asymmetric broad peaks, and, with the increasing of Ce^{3+} content, the energy transfer of intra-Ce^{3+} becomes to be significant, this kind

energy transfer that also leads to red shift and broader of emission and excitation spectra [32].

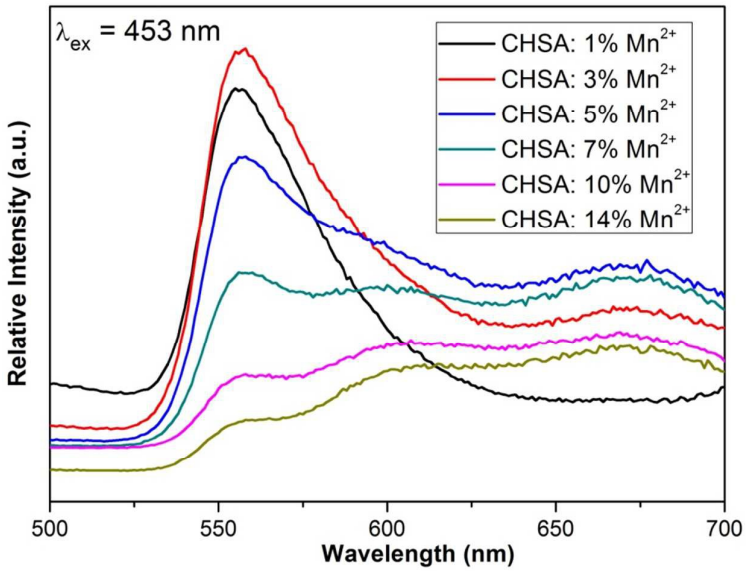

Figure 5 PL properties under 453 nm excitation of series $Ca_3Hf_2SiAl_2O_{12}$: *y*%Mn^{2+} phosphors

The PL spectra of $Ca_3Hf_2SiAl_2O_{12}$: *y*%Mn^{2+} with different Mn^{2+} content are shown in Figure 5. With 453 nm excitation, CHSA: Mn^{2+} can emit visible light which attributes $^4T_1(^4G)$–$^6A_1(^6S)$ transition of the Mn^{2+}. Specially, in the low content, it is clearly that CHSA: Mn^{2+} can emit green light peaking at about 556 nm. With the increasing of Mn^{2+} content, another two peaks appear peaking at about 590 and 670 nm and emit orange and red light. According to above site occupying situations of Mn^{2+}, the special emission spectra of CHSA: Mn^{2+} can be explained by different occupying site of Mn^{2+}. In the low content of Mn^{2+}, Mn^{2+} may substitute Al^{3+}/Si^{4+} site. Generally speaking, the emission properties of Mn^{2+} are determined to the coordination number of the occupied site in the crystal structure mainly by Mn^{2+} [33, 34]. With the coordination number increasing, the emission of Mn^{2+} will shift to red range in the spectra. In this CHSA structure, Al^{3+}/Si^{4+} are four coordinations. That is a relative small coordination and when Mn^{2+} occupies in this site, it will emit shortwave light. Therefore, in the low content of Mn^{2+} it will emit green light in this system. The occupying situation of Mn^{2+} in low content is certified by XRD peaks shift and emission spectra property. Furthermore, in high content of Mn^{2+} another two emission peaks appear. We conjecture that in high Mn^{2+} content, Mn^{2+} will occupy Hf^{4+} and Ca^{2+} site. Due to different coordination of Hf^{4+} and Ca^{2+}, when Mn^{2+} occupy these two sites it will emit different light. Hf^{4+} has six coordinations and Ca^{2+} is eight as shown in Figure 1. Therefore, when Mn^{2+} substitutes Hf^{4+} site it will emit orange light peaking at 590 nm while Mn^{2+} substitutes Ca^{2+} site it will emit orange light peaking at 670 nm, respectively. According to emission spectra properties, we conjecture that Mn^{2+} may substitute both Hf^{4+} and Ca^{2+}. That can be as a supportive certification of Mn^{2+} occupying situation in high content.

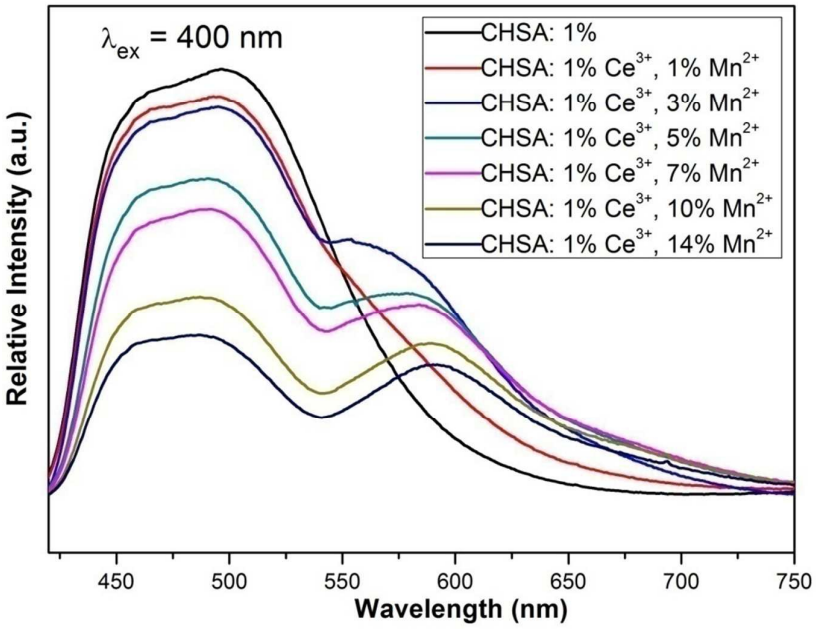

Figure 6 PL spectra of $Ca_3Hf_2SiAl_2O_{12}$: 1%Ce^{3+}, *y*%Mn^{2+} phosphors on Mn^{2+} doping concentration (y) (λ_{ex} = 360 nm).

The PL properties of Ce-Mn co-doped CHSA phosphors are shown in Figure 6. It is clearly seen that the spectra are consist of two parts, one is at the range of 450-525 nm which can be attributed to Ce^{3+} emission; another part is at about 550-650 nm, which can be attributed to Mn^{2+} emission. Furthermore, as the general situation, with the increasing of Mn^{2+} content, the intensities of Ce^{3+} emission are decreasing gradually and the intensities of Mn^{2+} are increasing, respectively. More importantly, in the Ce-Mn co-doped situation, in the low Mn^{2+} content, specially, at 3%, the intensity of emission peaking at 556 nm reaches to highest. With the increasing of Mn^{2+} content, the emission peaking at 556 nm becomes weak and disappears in the spectra cause to concentration quenching and anther peak at 590 nm appear and then becomes weak. The emission peaks of Mn^{2+} just appear two peaking at about 556 and 590 nm which is different with the Mn^{2+} single-doped phosphor shown in Figure 5. We surmise that the different energy transition efficiency between Ce^{3+} and Mn^{2+} may lead to this special situation. In general, the resonant-type energy transfer from a sensitizer to an activator in a phosphor may take place via the exchange interaction and electric multipolar interaction. In many cases, concentration quenching is due to energy transfer from one activator to another until an energy sink in the lattice is reached. The critical distance R_C for energy transfer from the Ce^{3+} to Mn^{2+} ions can be calculated using the concentration quenching method. According to Blasse, the critical distance R_C can be described by [35]

$$R_c \approx 2\left(\frac{3V}{4\pi x_c N}\right)^{1/3}$$

Where N is the number of available sites for the dopant in the unit cell, x_c is the total concentration of the Ce^{3+} and Mn^{2+} ions, and V is the volume of the unit cell. According to previous study on the crystal structure of CHSA, the acquired values 1891.26 $Å^3$, respectively. N has different values cause to different occupying situation of Mn^{2+}. There are three possible situations: (1) when Mn^{2+} occupies Al^{3+}/Si^{4+}, N_1 is 72; (2) when Mn^{2+} occupies Hf^{4+}, N_2 is 71; (3) when Mn^{2+} occupies Ca^{2+},

N_3 is 36. After calculation, the values of R_c in three situations are R_{c1}=10.8 Å, R_{c2}=10.1 Å and R_{c3}=12.6 Å. According to the results, we find that $R_{c1}\approx R_{c2}$ and they are smaller than R_{c3} which demonstrates that when Mn^{2+} occupies Al^{3+}/Si^{4+} and Hf^{4+} it has smaller critical distance. The smaller critical distance leads to more chances for Ce^{3+} to transfer energy to Mn^{2+}. This result leads to the two emission peaks (556 and 590 nm) of Mn^{2+} in co-doped CHSA phosphor appear and the third peak at 670 nm obtains little energy from Ce^{3+} and too weak and does not appearing in co-doped emission spectra.

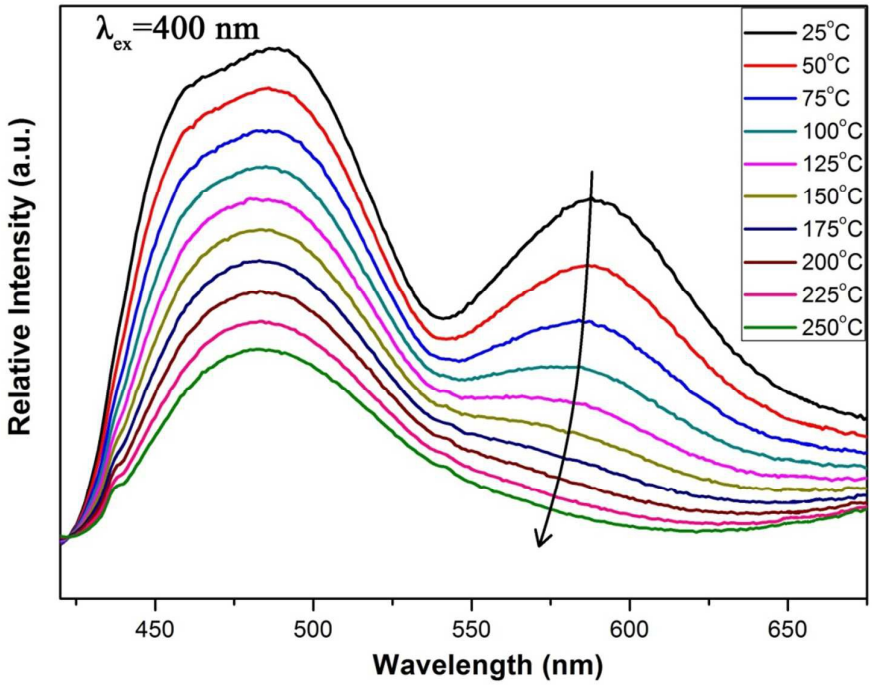

Figure 7Temperature dependence of $Ca_3Hf_2SiAl_2O_{12}$: 1%Ce^{3+}, 14%Mn^{2+} PL properties

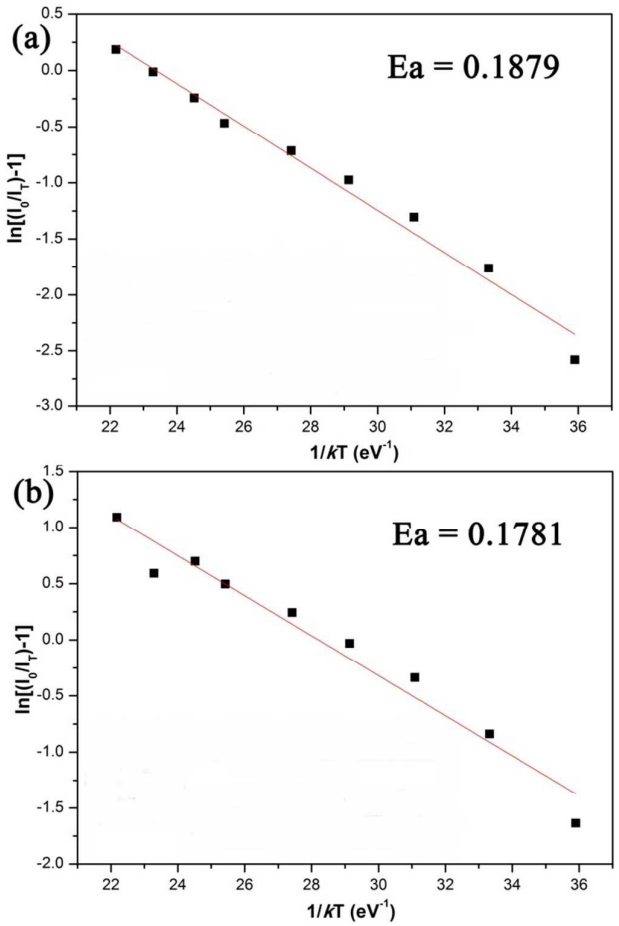

Figure 8 The Arrhenius fitting of the emission intensity of $Ca_3Hf_2SiAl_2O_{12}$: 1%Ce^{3+}, 14%Mn^{2+}phosphor and the calculated Ea for thermal quenching at Ce^{3+} (a) and Mn^{2+} (b) emission.

Temperature-dependent relative emission intensity under 400 nm excitation of CHSA: 1%Ce^{3+}, 14%Mn^{2+} is indicated in Figure 7. It can be clearly seen that with temperature increasing, the emission intensity decreases gradually and the emission band of Ce^{3+} goes from two apparent asymmetric broad peaks to one broad band definitely. Generally, the thermal quenching of emission intensity can be explained by a configurational coordinate diagram in which, through phonon interaction, the excited luminescence center is thermally activated through the crossing point between the excited state and the ground state. This non-radiative transition probability by thermal activation is strongly dependent on temperature resulting in the decrease of emission intensity [36, 37]. Due to the increasing phonon interaction and non-radiative transition with increasing temperature, the spectral overlap between the excitation band (Figure 3b) and the first emission band (5d-$^2F_{5/2}$ emission band) increases. This results in more re-absorption of the first emission due to the 5d-$^2F_{5/2}$ transition and thus in a relative stronger decrease of the 458 nm with respect to the 486 nm emission band. That leads to two apparent asymmetric broad peaks to one broad band definitely with temperature increasing. Furthermore, the Mn^{2+} emission spectra also take on a slight blue shift with temperature increasing. A similar phenomenon has been found and studied in other Mn^{2+} ion doped phosphors [38]. It was ascribed to the thermally active phonon-assisted tunnelling from the excited states of the lowenergy emission band to the excited states of the high-energy emission band in the configuration coordinate diagram. In order to better

understand temperature dependence of the luminescence, the activation energy (Ea) was calculated using the Arrhenius equation [39]

$$I_T = \frac{I_0}{1+c\exp(-\frac{\Delta E}{kT})}$$

where I_0 is the initial PL intensity of the phosphor at room temperature, I_T is the PL intensity at different temperatures, c is a constant, ΔE is the activation energy, and k is the Boltzmann constant (8.62×10^{-5} eV). Making this function to do logarithmic transformation can get [40]

$$\ln\left(\frac{I_0}{I_T} - 1\right) = c(-\frac{\Delta E}{kT})$$

According to the equation, the activation energy ΔE can be calculated by plotting $\ln[(I_0/I_T)-1]$ against $1/kT$, where a straight slope equals ΔE. As shown in Figure 8, ΔE of Ce^{3+} emission was found to be 0.1879eV and 0.1781eV for Mn^{2+} emission.

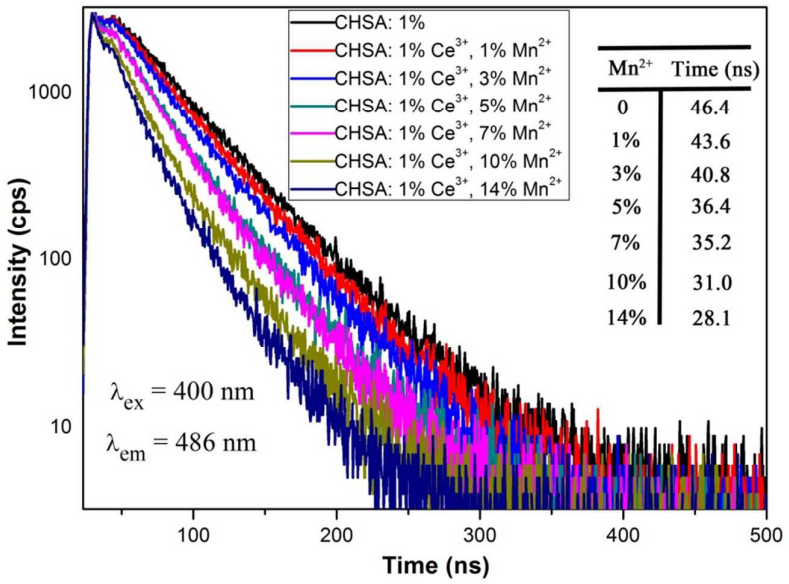

Figure 9 Decay curves of $Ca_3Hf_2SiAl_2O_{12}$: 1%Ce^{3+}, y%Mn^{2+} phosphors with different Mn^{2+} contents

The PL decay curves of CHSA: 1%Ce^{3+}, $y$$Mn^{2+}$ excited at 400 nm and monitored the main emission of the Ce^{3+} ions at 486 nm were measured, and the lifetimes are shown in Fig. 9. It can be seen that the decay curves of the 5d–4f transition of CHSA: 1%Ce^{3+}, $y$$Mn^{2+}$ shows a second order exponential decay, which can be fitted by the equation [41]:

$$I(t) = A_1 \exp(-t/\tau_1) + A_2 (-t/\tau_2)$$

Where I is the luminescence intensity; A_1 and A_2 are constants; t is time; and τ_1 and τ_2 are the lifetimes for the exponential components. Further, the average lifetime constant (τ^*) can be calculated as:

$$\tau^* = (A_1\tau_1^2 + A_2\tau_2^2)/(A_1\tau_1 + A_2\tau_2)$$

The calculated average lifetimes of CHSA: 1%Ce^{3+}, $y$$Mn^{2+}$ (y = 1%, 3%, 5%, 7%, 10%, 14%) are 43.6, 40.8, 36.4, 35.2, 31.0 and 28.1 ns, respectively. The decay time of CHSA: 1%Ce^{3+} sample without the Mn^{2+} was determined to be 46.4 ns for the 5d–4f transition. However, when the Mn^{2+} was doped in the system of CHSA: 1%Ce^{3+}, the decay of Ce^{3+} ions becomes faster and faster. The decay time of the Ce^{3+} ions was found to decrease as the Mn^{2+} concentrations increases, which

demonstrates that the energy transfer process occurs from sensitizer Ce^{3+} to activator Mn^{2+}. Additional, the energy transfer efficiency from Ce^{3+} to Mn^{2+} in CHSA matrix can be determined using the calculation below:

$$\eta_T = 1 - \frac{\tau_x}{\tau_0}$$

Where τ_0 and τ_x stand for the lifetimes of the sensitizer Ce^{3+} in the absence and the presence of activator Mn^{2+}, respectively. The energy transfer efficiency was calculated to be 6%, 12%, 21%, 24%, 33% and 39%. The energy transfer efficiency is found to increase with increasing Mn^{2+} content. When the doped Mn^{2+} concentration was 14%, the value of energy transfer efficiency is estimated to be 39%. So, it indicated that the Mn^{2+} emission intensity was enhanced via energy transfer from sensitizer Ce^{3+}, instead of the energy absorption by Mn^{2+} ions themselves.

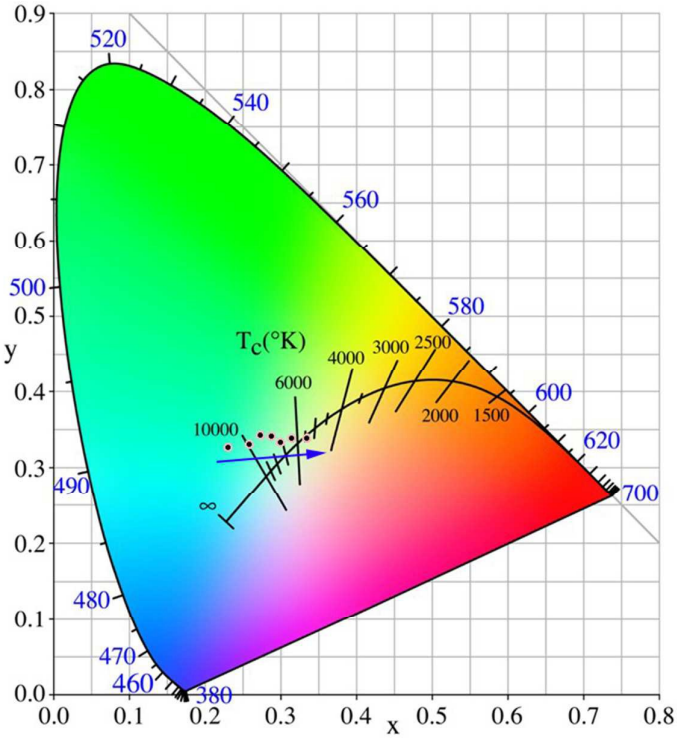

Figure 10 CIE chromaticity diagram and coordinate of $Ca_3Hf_2SiAl_2O_{12}$: 1%Ce^{3+}, *y*%Mn^{2+} (*y*=0-14) phosphors

Table 1 Comparison of the CIE chromaticity coordinates (x, y) for CHSA: 1%Ce^{3+}, *y*Mn2+ phosphors excited at 400 nm

Ce^{3+}(x) and Mn^{2+}(y) content	CIE coordinates (x, y)	Color temperature (K)
x=1%, y=0	(0.2303, 0.3265)	12763 K
x=1%, y=1%	(0.2593, 0.3302)	10005 K
x=1%, y=3%	(0.2735, 0.3431)	8628 K
x=1%, y=5%	(0.2882, 0.3413)	7768 K
x=1%, y=7%	(0.2994, 0.3332)	7224 K
x=1%, y=10%	(0.3148, 0.3381)	6345 K
x=1%, y=14%	(0.3350, 0.3388)	5379 K

The variation of the Commission International de L'Eclairage (CIE) chromaticity coordinates and color temperature of the CHSA: 1%Ce^{3+}, *y*Mn^{2+} phosphors with different doping contents of Mn^{2+}

are calculated based on the corresponding PL spectrum upon 400 nm excitation summarized in Fig. 10 and Table 1. Increasingly, the color tune can be modulated from cyan (0.2303, 0.3265) to white (0.3350, 0.3388) with the increasing doping content of the Mn^{2+} ions, which is due to the variation of the emission intensity of Ce^{3+} and Mn^{2+} through the energy transfer from Ce^{3+} to Mn^{2+}. The correlated color temperature can be adjusted from 12763 K to 5379 K. The emission color is tunable in the visible region from blue to white by controlling Mn^{2+} doped contents which indicates that the series of CHSA: 1%Ce^{3+}, *y*Mn^{2+} phosphors are promising candidates for color tunable luminescence material used for the n-UV w-LEDs.

4. Conclusions

In summary, a series of color-adjustment CHSA: Ce^{3+}, Mn^{2+} phosphors were prepared through a conventional solid-state reaction. It was found that three different cation sites (Ca^{2+}, Hf^{4+} and Al^{3+}/Si^{4+}) in the $Ca_3Hf_2SiAl_2O_{12}$ phase were occupied evenly by Ce^{3+} and Mn^{2+} ions. Different situation of Mn^{2+} occupying sites and energy transfer from Ce^{3+} to Mn^{2+} can appear with different Mn^{2+} content and the critical distance was calculated to be R_{c1}=10.8 Å, R_{c2}=10.1 Å and R_{c3}=12.6 Å after calculation of energy transfer from the Ce^{3+} to Mn^{2+} by using the concentration quenching method. $Ca_3Hf_2SiAl_2O_{12}$: Ce^{3+}, Mn^{2+} phosphors exhibited a broad excitation band ranging from 300 to 450 nm and two broad asymmetric emission bands upon 400 nm excitation. The emission color of the obtained phosphors can be modulated from blue-green (0.2303, 0.3265) to white (0.3350, 0.3388) by controlling the doping content of the Mn^{2+} ions with the fixed Ce^{3+} content. The correlated color temperature can be adjusted from 12763 K to 5379 K.

Acknowledgment

This work is supported by Specialized Research Fund for the Doctoral Program of Higher Education (no. 20120211130003), State Key Laboratory on Integrated Optoelectronics (No. IOSKL2013KF15).

Reference

[1] S. Ye, F. Xiao, Y. X. Pan, Y. Y. Ma, Q. Y. Zhang, *Mater. Sci. Eng. R.* 2010, **71**, 1

[2] A. Kitai, *John Wiley & Sons, Ltd ISBN,* **2008**, 978-0-470-05818-3

[3] W. B. Im, N. George, J. Kurzman, S. Brinkley, A. Mikhailovsky, J. Hu, B. F. Chmelka, S. P. DenBaars, R. Seshadri, *Adv. Mater*. 2011, **23**, 2300

[4] Y. Shimomura, T. Honma, M. Shigeiwa, T. Akai, K. Okamoto, N. Kijima, *J. Elect. Soc.* 2007 **154**, 35

[5] A. A. Setlur, W. J. Heward, Y. Gao, A. M. Srivastava, R. G. Chandran, M. V. Shankar, *Chem. Mater.* 2006, **18**, 3314

[6] J. K. Li, J.G. Li, S.H. Liu, X. D. Li, X. D. Sun, O. Sakkab, *J. Mater. Chem. C*. 2013, **1**, 7614

[7] J. M. Phillips, M. E. Coltrin, M. H. Crawford, A. J. Fischer, M. R. Krames, R. M. Mach, G. O. Mueller, Y. Ohno, L. E. S. Rohwer, J. A. Simmons, J. Y. Tsao, *Laser & Photon. Rev.* 2007, ***1*, *4***, 307

[8] W. B. Im, S. Brinkley, J. Hu, A. Mikhailovsky, S. P. Denbaars, R. Seshadri, *Chem. Mater.* 2010, **22,** 2849

[9] C. K. Chang, T. M. Chen, *Appl. Phys. Lett.* 2007, **90,** 161901

[10] C. M. Liu, Z. M. Qi, C. G. Ma, P. Dorenbos, D. J. Hou, S. Zhang, X. J. Kuang, J. H. Zhang, H. B. Liang, *Chem. Mater*. 2006, **18,** 3709

[11] Z. G. Xia, J. Zhou, Z. Y. Mao, *J. Mater. Chem. C*, 2013**, 1,** 5917

[12] C. Y. Liu, Z.G. Xia, Z. P. Lian, J. Zhou, Q. F. Yan, *J. Mater. Chem. C*, 2013, **1,** 7139

[13] D. G. Deng, H. Yu, Y.Q. Li, Y. J. Hua, G. H. Jia, S. L. Zhao, H. P. Wang, L. H. Huang, Y. Y. Li, C. X. Li, S. Q. Xu, *J. Mater. Chem. C*, 2013**, 1,** 3194
[14] S. H. Miao, Z. G. Xia, M. S. Molokeev, M. Y. Chen, J. Zhang and Q. L. Liu, *J. Mater. Chem. C*, 2015, 3, 4616
[15] H. K. Park, J. H. Oh, H. Kang, J. Zhang, and Y. R. Do, *Appl. Mater. Interfaces* 2015, **7**, 4549
[16] W. B. Park, S. P. Singh, M. Kim and K. S. Sohn, *Inorg. Chem.* 2015, **54**, 1829
[17] V. Bachmann, C. Ronda, and A. Meijerink, *Chem. Mater.* 2009, **21**, 2077
[18] H. K. Liu, L. B. Liao and Z. G. Xia, *RSC Adv.*, 2014, **4**, 7288
[19] T. Ishigaki, A. Torisaka, K. Nomizu, P. Madhusudan, K. Uematsu, K. Toda M. Satoac, *Dalton Trans.*, 2013, **42**, 4781
[20] Y. C. Jia, Y. J. Huang, N. Guo, H. Qiao, Y. H. Zheng, W. Z. Lv, Q. Zhao, H. P. You, *RSC Advances*, 2012, **2**, 2678
[21] C. Bertail, S. Maron, V. Buissett, T. L. Mercier, T. Gacoin, J. P. Boilot, *Chem. Mater.* 2011, **23**, 2961
[22] W. B. Dai, S. Ye, E. L. Li, P. Z. Zhuo, Q. Y. Zhang, *J. Mater. Chem. C*, 2015, **3**, 8132
[23] W. J. Tang, Z. Zhang, *J. Mater. Chem. C*, 2015, **3**, 5339
[24] Y. F. Liu, X. Zhang, Z. D. Hao, X. J. Wang and J. H. Zhang, Chem. Commun., 2011, 47, 10677.
[25] X. G. Zhang and M. L. Gong, Mater. Lett., 2011, 65, 1756.
[26] G. G. Li, D. L. Geng, M. M. Shang, C. Peng, Z. Y. Cheng and J. Lin, J. Mater. Chem., 2011, 21, 13334.
[27] C. H. Huang and T. M. Chen, J. Phys. Chem. C, 2011, 115, 2349.
[28] I. O. Galuskina, E. V. Galuskin, K. Prusik, V. M.Gazeev, N. N. Pertsev, P. Dzierzanowski, *Miner. Magaz.* 2013, **7(6)**, 2857
[29] I. O. Galuskina, E.V. Galuskin, P. Dzierżanowski, V. M. Gazeev, K. Prusik, N. Pertsev, A. Winiarski, A. E. Zadov, R. Wrzalik, *Am. Miner.* 2010, **95,** 1305
[30] H. S. Jang, Y. H. Won, D.Y. Jeon, *Appl. Phys. B* 2009, **95,** 715
[31] S. H. Miao, Z. Z. Xia, M. S. Molokeev, M. Y. Chen, J. Zhan, Q. Liu, *J. Mater. Chem. C*, 2015, 3, 4616
[32] W. Y. Huang, F. Yoshimura, K. Ueda, Y. Shimomura, H. S. Sheu, T. S. Chan, C. Y. Chiang, W. Z. Zhou, R. S. Liu, *Chem. Mater.*, 2014, **26 (6)**, 2075
[33] P. Pust, V. Weiler, C. Hecht, A. Tücks, A. S. Wochnik, A. K. Henß, D. Wiechert, C. Scheu, P. J. Schmidt, W. Schnick, *Nat. Mater.* 2014, **13**, 891
[34] Y. Q. Li, N. Hirosaki, R. J. Xie, T. Takeda, M. Mitomo, *Chem. Mater.* 2008, **20,** 6704
[35] Y. Sato, H. Kato, M. Kobayashi, T. Masaki, D. H. Yoon, M. Kakinada, *Angew. Chem. Int. Ed.* 2014, **53**, 7756.
[36] J. F. Sun, Z. P. Lian, G. Q. Shen, D. Z. Shen, *RSC Adv.* 2013, **3**, 18395.
[37] R. D. Shannon, *Acta Cryst.*, 1976, **A32**, 751.
[38] C. Y. Liu, Z. G. Xia, Z. P, Lian, J. Zhou, Q. F. Yan, *J. Mater. Chem. C*, 2013, **1**, 7139.
[39] W. Z. Lv, Y. C. Jia, Q. Zhao, W. Lu, M. M. Jiao, B. q. Shao, H. P. You, *J. Phys. Chem. C*, 2014, **118**, 4649.
[40] S. P. Lee, C. H. Huang, T. S. Chan, T. M. Chen, *Appl. Mater. Interfaces.* 2014, **6 (10)**, 7260.
[41] D. A. McKeown, A. C. Nobles, *Phys. Rev.* 1996, **B 54**, 291308

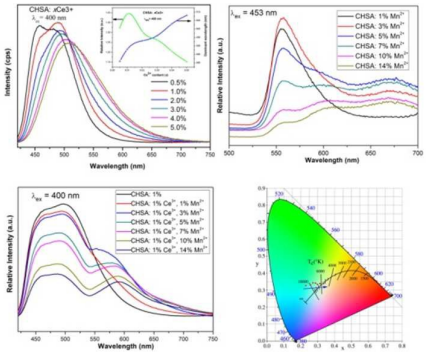

A series of color-adjustable phosphors $Ca_3Hf_2SiAl_2O_{12}:Ce^{3+}$, Mn^{2+} were synthesized. Its Structure, luminescence property and abnormal energy transfer behavior were investigated.